Talanta 198 (2019) 417–423

Contents lists available at ScienceDirect

Talanta

journal homepage: www.elsevier.com/locate/talanta

Facile fabrication of visible light photoelectrochemical immunosensor for SCCA detection based on $BiOBr/Bi_2S_3$ heterostructures via self-sacrificial synthesis method

Dawei Fan*, Chunzhu Bao, Xin Liu, Jinhui Feng, Dan Wu, Hongmin Ma, Huan Wang, Qin Wei, Bin Du

Key Laboratory of Interfacial Reaction & Sensing Analysis in Universities of Shandong, School of Chemistry and Chemical Engineering, University of Jinan, Jinan 250022, PR China

ARTICLE INFO

Keywords:
BiOBr
Bi_2S_3
Self-sacrificial synthesis method
Visible light
Photoelectrochemical immunosensor

ABSTRACT

A novel visible light photoelectrochemical immunosensor based on $BiOBr/Bi_2S_3$ heterostructures was fabricated to detect squamous cell carcinoma antigen (SCCA). Bi_2S_3 nanoparticles formed on the BiOBr microflowers by the self-sacrificial synthesis method based on the facile reaction between BiOBr and S^{2-} ions. The $BiOBr/Bi_2S_3$ composites exhibited excellent visible light photoelectrochemical activity, when ascorbic acid (AA) was employed as a perfect electron donor. The photocurrent intensity of $BiOBr/Bi_2S_3$ modified ITO electrode arrived at around 20 μA, which was approximately 30 times than that of pure BiOBr. Dopamine formed easily polydopamine film via self-polymerization on the surface of $BiOBr/Bi_2S_3$ composites to immobilize SCCA antibody. Under the optimal condition, this photoelectrochemical immunosensor realized the ultrasensitive determination of SCCA. With the logarithm of SCCA concentration in the range of 0.001–75 ng mL^{-1}, the specific binding between SCCA and antibody led to the linearly decrease of photocurrent signal with a low detection limit of 0.3 pg mL^{-1} (S/N = 3). This facilely constructed photoelectrochemical immunosensor maybe have promising practical application in photocatalysis, analytical detection and biosensor, etc.

1. Introduction

With the high morbidity and mortality, lung cancer increasingly threatens the health of people. Therefore, exploring effective tumor markers is crucial. According to the previous reports, Tong et al. studied the application of squamous cell carcinoma antigen (SCCA) in the diagnosis of lung cancer [1]. They found that SCCA was related with the development condition of lung cancer, which can be used to detect the clinically recurrence and metastasis of malignant tumors. Zhao et al. found that the content of SCCA was significantly increased in the lung cancer group [2]. And the level of squamous cell carcinoma was higher than other pathological types of lung cancer, suggesting that SCCA played an important role in the determination of the pathological types of lung cancer. Therefore, SCCA is generally applied as a dependable tumor marker for the early diagnosis of lung cancer [3–5].

Nowadays, photoelectrochemical (PEC) immunosensor has been extensively focused in the fields of analysis and detection [6–9]. PEC immunosensor detects target accurately by transforming light signals into electrical signals, and possesses many advantages, such as strong specificity, fast analysis speed, high accuracy, simple operating system and excellent selectivity for the target [10–13]. Therefore, a novel and facile visible light PEC immunosensor is fabricated to detect SCCA in our work. As the crucial factor of the preparation of PEC immunosensor, the selection of PEC material needs to be carefully treated, which is benefit to enhancing the sensitivity of PEC immunosensor.

Recently, as a typical p-type semiconductor material, bismuthyl bromide (BiOBr) has attracted significant interest in various fields, such as photocatalytic activity [14], sensor [9], electrocatalytic alcohol oxidation [15] and so on. BiOBr has unique and excellent electrical, magnetic and optical properties, such as excellent chemical stability, good photoelectric activity and suitable band-gap [16–18]. The wide band-gap of BiOBr about 2.7 eV could inhibit the recombination of electron-hole (e^-/h^+), which is benefit to the strengthening of photoelectric activity. According to the previous references, the photoelectric activity of BiOBr is diverse due to their different morphology, for example, 2-dimensional flaky structure, 3-dimensional floral structure, hollow microspheres and spherical microflowers [19]. In our work, the BiOBr with hierarchical microsphere structure is prepared by

* Corresponding author.
E-mail address: jndxfandawei@126.com (D. Fan).

https://doi.org/10.1016/j.talanta.2019.02.043
Received 19 September 2018; Received in revised form 1 January 2019; Accepted 9 February 2019
Available online 10 February 2019
0039-9140/

hydrothermal synthesis method. The smooth surface and the larger specific surface of BiOBr increase the binding sites, promoting the combination of BiOBr with more particles.

Moreover, the construction of heterojunction is an effective technique to improve the photoelectric activity of PEC immunosensor. For example, Guo et al. prepared BiOBr/Bi heterojunctions [20], Hu et al. fabricated a Z-scheme Bi_2MoO_6/BiOBr photocatalyst [21], Di et al. prepared N-CQDs/BiOBr [22]. Recently, bismuth sulfide (Bi_2S_3) with a narrow band-gap (1.30–1.70 eV) has attracted intensive attention in the fields of photocatalytic degradation [23], electrochemical determination [24] and so on. The most important thing is that the valence band (VB) and conduction band (CB) of Bi_2S_3 are higher than that of BiOBr. The satisfying match of band-gap accelerates efficiently the electron transfer under the visible light irradiation, which improves the conductivity of PEC immunosensor. Therefore, as the matrix, the BiOBr/Bi_2S_3 heterostructures were fabricated via self-sacrificial synthesis method in our work.

Most importantly, it is the first time that Bi_2S_3 nanoparticles formed on the BiOBr microflowers by the self-sacrificial synthesis method. Comparing with other references [25–28], the self-sacrificial synthesis method is simple and quick. The obtained BiOBr/Bi_2S_3 composites exhibit excellent photoelectric activity, when ascorbic acid (AA) is employed as a perfect electron donor. Based on the above discussion, a novel visible light PEC immunosensor based on BiOBr/Bi_2S_3 heterostructures is designed via self-sacrificial synthesis method to detect SCCA.

2. Experimental

2.1. Materials and instrumentation

SCCA and SCCA antibodies (anti-SCCA) McAb (coating) were purchased from Shanghai Linc-Bio Science Co., Ltd. China. Tris(hydroxymethyl)aminomethane was purchased from Shanghai Macklin Biochemical Co., Ltd. China, which was used for the preparation of Tris-HCl buffer solution. X-ray photoelectron spectroscopy (XPS) analysis was performed on ESCALAB 250 X-ray photoelectron spectrometer (Thermo Fisher Scientific, USA). The other details are shown in Electronic Supplementary Information (ESI†)

2.2. Preparation of hierarchical BiOBr microspheres

The hierarchical BiOBr microspheres were fabricated by a typical synthetic procedure according to the report [29]. Under the magnetic stirring, $Bi(NO_3)_3{\cdot}5H_2O$ (4 mmol) was dissolved in 2-methoxyethanol (80 mL) as solution A. Analogously, 1-dodecyl-3-methylimidazolium bromide ($[C_{12}Mim]Br$), 6 mmol) was injected into 80 mL of 2-methoxyethanol as solution B. The above solution A and B were mixed together and magnetically stirred for 10 min. Then the mixed solution was transferred into an autoclave (100 mL) to react at 160 °C for 2 h. After cooling to room temperature, the product was centrifuged and washed three times with ethanol and ultrapure water, respectively. Finally, the product was dried in vacuum to obtain the hierarchical BiOBr microsphere.

2.3. Fabrication of PEC immunosensor

As shown in Fig. 1, the PEC immunosensor was prepared by layer-by-layer (LBL) assembly. Before fabrication, the ITO substrates (3.0 × 0.8 cm^2) were processed by ultrasound in acetone, ethanol and ultrapure water for 30 min, respectively. After drying, the ITO slices were reserved to use. Firstly, 4 mg mL^{-1} of BiOBr (10 μL) were coated on ITO, and then calcinated in muffle furnace at 400 °C for an hour. After cooled to room temperature, Na_2S solution (5 μL) was modified on the ITO/BiOBr electrode. By self-sacrificial synthesis method, Bi_2S_3 generated on the BiOBr microspheres due to the reaction between S^{2-} and

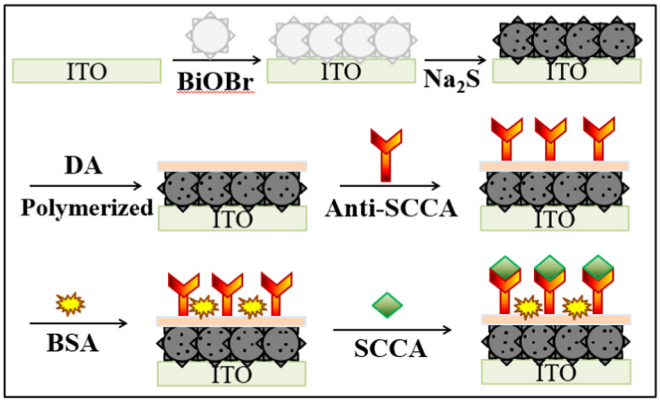

Fig. 1. The schematic of the preparation process of PEC immunosensor.

BiOBr. Subsequently, the prepared ITO/BiOBr/Bi_2S_3 electrode was rinsed with ultrapure water to remove redundant Na_2S. Then, 5 μL of dopamine hydrochloride (1 mg mL^{-1}) in pH 8.5 Tris-HCl solution was modified on the above electrode for one hour and then cleaned with ultrapure water. It is effortless for dopamine hydrochloride (DA) to polymerize, which makes it possess the excellent adsorptivity. The polydopamine film (PDA) formed by self-aggregation not only consolidated the stability of photoelectric signals, but also facilitated the binding of anti-SCCA. Anti-SCCA (10 μg mL^{-1}, 5 μL) was added to the ITO/BiOBr/Bi_2S_3/PDA electrode and incubated at room temperature. Followed by washing the uncombined anti-SCCA, BSA (5 μL, 1 mg mL^{-1}) was dropped onto ITO/BiOBr/Bi_2S_3/PDA/anti-SCCA electrode to block the nonspecific binding sites. After rinsing, different concentrations of SCCA (5 μL) was modified on the ITO/BiOBr/Bi_2S/PDA/anti-SCCA/BSA electrode, respectively. Finally, rinsed with ultrapure water, the ITO/BiOBr/Bi_2S_3/PDA/anti-SCCA/BSA/SCCA PEC immunosensor was prepared successfully by LBL assembly.

3. Results and discussion

3.1. Characterization of BiOBr, and BiOBr/Bi_2S_3

As shown in Fig. 2, the morphology and elemental analysis of the prepared BiOBr, and BiOBr/Bi_2S_3 were researched by scanning electron microscope (SEM) and energy dispersive spectrometry (EDS). The SEM (Fig. 2A) and magnified SEM (Fig. 2B) images of BiOBr coated on ITO without calcination indicated that BiOBr has a complete hierarchical microsphere structure. BiOBr has a smooth surface, which like blooming petals. And the larger specific surface increased the binding sites, promoting the combination of BiOBr with more particles. Moreover, the existence of Bi, O and Br elements in EDS image of BiOBr without calcination (Fig. 2C) convincingly confirmed the successful fabrication of hierarchical BiOBr microsphere. In order to enhance the combination between BiOBr and ITO, the BiOBr coated on ITO was calcined in muffle furnace at 400 °C for an hour, and the SEM and magnified SEM images of calcined BiOBr coated on ITO were further surveyed (Fig. S1). Compared the SEM of BiOBr before and after calcination, there was no obvious change in morphology and the calcinated BiOBr possessed more satisfactory aggregation. Based on the calcination, Na_2S solution was modified on the BiOBr coated ITO to obtain the BiOBr/Bi_2S_3 composites. Owing to the fact that the solubility product constant of BiOBr (3.0×10^{-7}) was much greater than that of Bi_2S_3 (4.97×10^{-47}), Bi_2S_3 was easier to form than BiOBr. Thus, after modifying Na_2S on ITO/BiOBr electrode, the S element in Na_2S could despoil Bi element in BiOBr to form Bi_2S_3 with excellent stability. Observing the SEM (Fig. 2D) and magnified SEM (Fig. 2E) images of BiOBr/Bi_2S_3, the surface of BiOBr/Bi_2S_3 composites was rough, and many particles attached to the surface of BiOBr microsphere. As shown

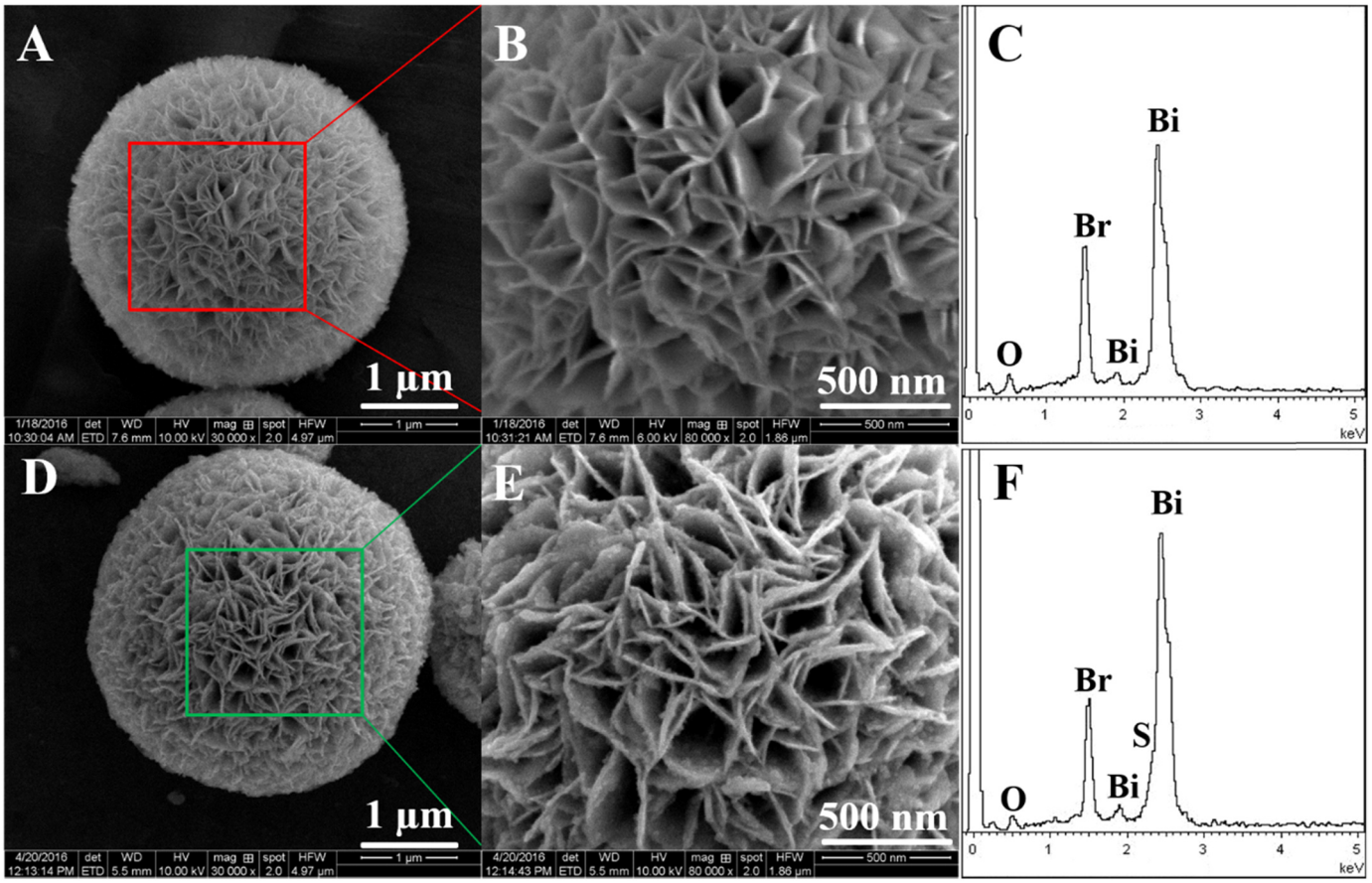

Fig. 2. SEM (A), magnified SEM (B) and EDS (C) images of BiOBr coated on ITO without calcination. SEM (D), magnified SEM (E) and EDS (F) images of calcined BiOBr/Bi_2S_3.

in Fig. 2F, it was obvious that Bi, O, Br and S element were existed in the EDS images of BiOBr/Bi_2S_3. By comparing the Tables S1 and S2 (ESI†), the EDS data indicated that the atom percentage of S was 5.88 in calcined BiOBr/Bi_2S_3 composites, which further improved the preparation of BiOBr/Bi_2S_3 was successful.

In order to prove the successful synthesis of materials, the X-ray diffraction (XRD) patterns of BiOBr and BiOBr/Bi_2S_3 were further studied in Fig. 3A. Through observing the XRD pattern of BiOBr, there was no other interferential diffraction peaks by comparing with the reference [29], which manifested the successful preparation of BiOBr. The diffraction peaks of BiOBr existed completely in the XRD pattern of BiOBr/Bi_2S_3. And the diffraction peaks of Bi_2S_3 were located at 22.4° and 34.0° revealing the successful loading of Bi_2S_3 [30]. It was worth mentioning that the low content of Bi_2S_3 leaded to the less diffraction peaks existed in the XRD pattern of BiOBr/Bi_2S_3.

The UV–vis diffuse reflectance spectra of BiOBr and BiOBr/Bi_2S_3 (Fig. 3B) exhibited the absorption effect of materials to visible light. It was obvious that the absorption wavelength range of pure BiOBr was mainly below 400 nm, which indicated that BiOBr had certain absorption of visible light (curve a). However, the absorption was weak in the visible light area. After interacted with Na_2S, the absorption of visible light enhanced obviously and the absorption area widened significantly, which proved that the BiOBr/Bi_2S_3 composite had distinguished photoelectric activity (curve b). The result could explain that Bi_2S_3, generated by self-sacrificial synthesis method, had narrow band-gap lead to the fewer required electron transition energy. Therefore, BiOBr/Bi_2S_3 composite could easily produce photo-generated electron-hole under visible light irradiation, causing the redshift of BiOBr absorption wavelength, which made the apparent increase of photoelectric activity. The insets in Fig. 3B were BiOBr coated ITO electrode (a) and Na_2S modified ITO/BiOBr electrode (b). After interacted with Na_2S, the color of the sample changed from white to black, certifying the formation of new substances. The color of Bi_2S_3 was black, which was consistent with the above explanation.

The X-ray photoelectron spectroscopy (XPS) spectra (Fig. 3C) displayed two obvious peaks at about 159.1 and 164.4 eV, which were resolved into Bi $4f_{7/2}$ and Bi $4f_{5/2}$ of Bi^{3+} in BiOBr, respectively. It is interesting that after interacting with Na_2S solution, the peak of O 1s changed from 530.0 eV to 529.8 and 531.2 eV (Fig. 3D). The two peaks could be explained to the bonding of Bi-O and O-H [31,32]. The XPS peaks of Br 3d of BiOBr/Bi_2S_3 in Fig. 3E shift to the higher binding energy than that of BiOBr, which were ascribed to the slight variation of the environment of Br 3d due to the heterostructure formation. As shown in Fig. 3F, there were two typical speaks at around 159.1 and 169.4 eV, which were consistent with the binding energy of S 2p, proving the successful generation of Bi_2S_3.

3.2. Optimization of experimental conditions

The concentrations of BiOBr, Na_2S and AA were optimized (shown in Fig. 4) to enhance the performance of the PEC immunosensor. Fig. 4A indicated that with the increase of BiOBr concentration, the intensity of photocurrent gradually enhanced in the range of 1–4 mg mL^{-1}. The phenomenon maybe explained that the thickness of the ITO/BiOBr electrode film could become larger as the increase of BiOBr concentration, which was benefit to the absorption of visible light and the generation of photo-generated electrons-holes. However, if the concentration of BiOBr was increased continually, the intensity of photocurrent could decrease due to the obstruction of thicker BiOBr film to the diffusion of electrons. Thus, the photocurrent reached the maximum

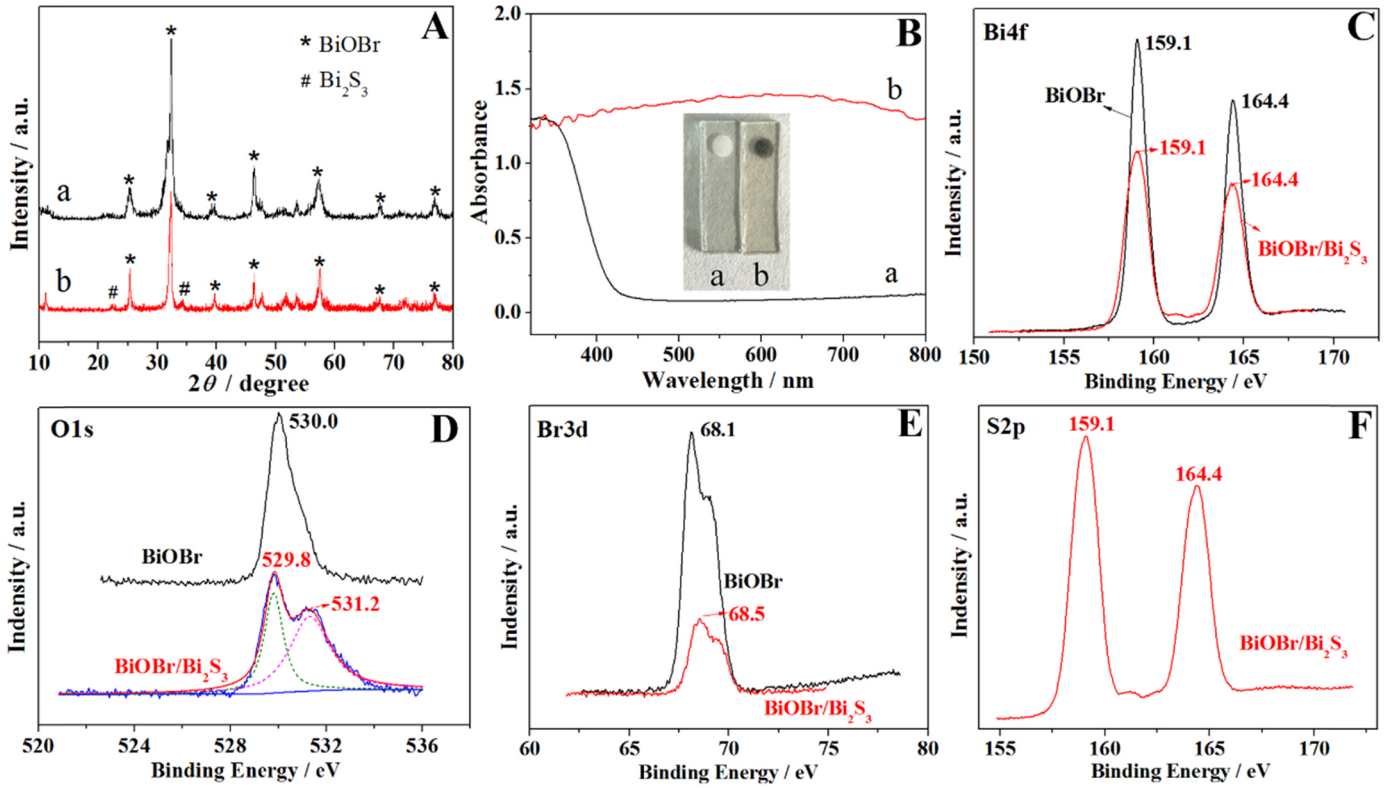

Fig. 3. (A) XRD patterns of BiOBr (a) and BiOBr/Bi_2S_3 (b). (B) UV–vis diffuse reflectance spectra of BiOBr (a) and BiOBr/Bi_2S_3 (b). The insets in B were BiOBr coated ITO electrode (a) and Na_2S modified ITO/BiOBr electrode (b). XPS spectra of BiOBr and BiOBr/Bi_2S_3, (C) Bi spectrum, (D) O spectrum, (E) Br spectrum, (F) S spectrum.

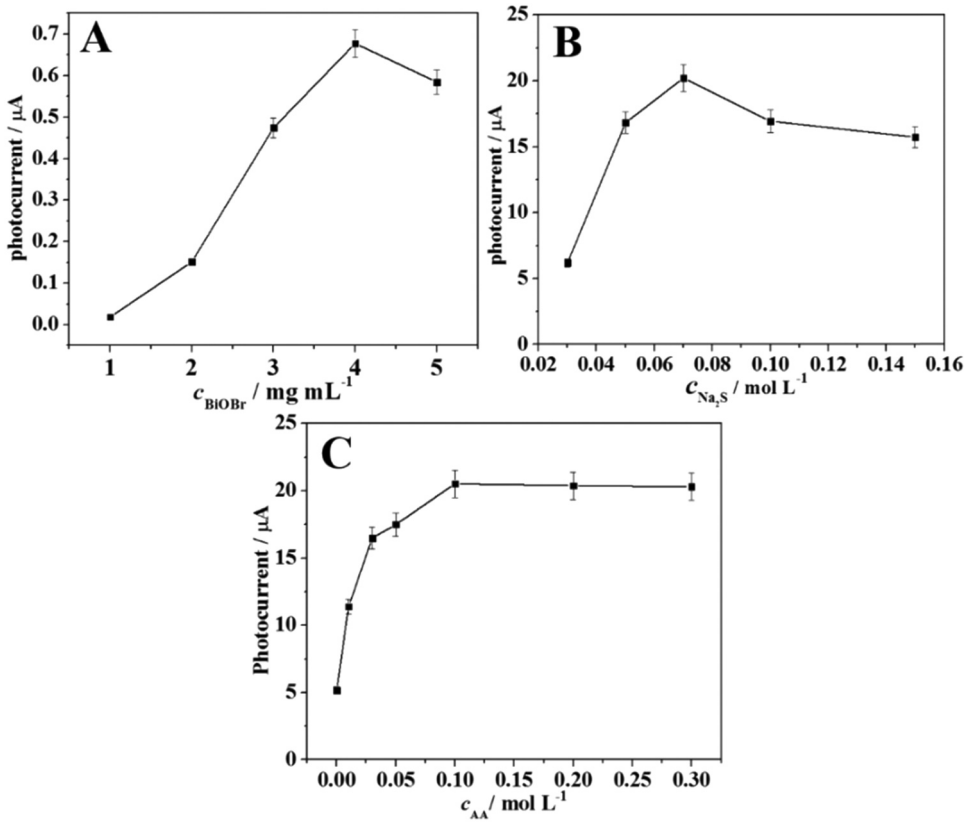

Fig. 4. Effects of concentrations of BiOBr on the photocurrent response of the ITO/BiOBr electrode (A). Effects of concentrations of Na_2S (B) and AA in the PBS buffer solution (C) on the photocurrent response of the ITO/BiOBr/Bi_2S_3 electrode. The potential was 0 V.

(0.68 μA) while the BiOBr concentration was 4 mg mL^{-1}. It was obvious that with the increase of the concentrations of Na_2S solution in the range of 0.03–0.07 mol L^{-1}, the intensity of photocurrent gradually enhanced (Fig. 4B). Nevertheless, as the increase of the concentrations of Na_2S, the photocurrent displayed a decreasing trend. The result could be explained that the amount of generated Bi_2S_3 was increased gradually, which contributed to the reinforcement of photoelectric activity. Once the concentration of Na_2S exceeded a certain range, the excess of Bi_2S_3 could block the electron transfer. So, the optimal concentration of Na_2S was designed as 0.07 mol L^{-1}. As shown in Fig. 4C, the intensity of photocurrent demonstrated an increasing trend until the concentration of AA achieved 0.10 mol L^{-1}, and then the intensity almost unchanged with the increase the concentration of AA. AA, as the excellent electron donor, could capture photo-generated holes to enhance the PEC activity. But, the electron donor could achieve saturation if the concentration of AA surpass 0.1 mol L^{-1}. Hence, the optimal concentration of AA was set as 0.1 mol L^{-1} in PBS buffer solution.

3.3. Characterization of the fabricated PEC immunosensor

Under the ideal condition, the time-based photocurrent response curves and electrochemical impedance spectroscopy (EIS) Nyquist plots of the fabricated PEC immunosensor were researched in Fig. 5. Firstly, Fig. 5A showed that the intensity of photocurrent corresponding bare electrode was nearly 0 μA (curve a). After modified with BiOBr, the intensity of photocurrent slightly rose to 0.68 μA (curve b). Fortunately, the ITO/BiOBr electrode coated with Na_2S manifested excellent photocurrent intensity (19.72 μA), which certified the BiOBr/Bi_2S_3 composite possess prominent PEC activity (curve c). In order to preferably combine with anti-SCCA, 1 mg mL^{-1} DA with distinguished adsorptivity was dropped on the ITO/BiOBr/Bi_2S_3 electrode to form PDA film. However, the loading of the organic layer not only prevented the electron transfer, but also weakened the irradiation of visible light to BiOBr/Bi_2S_3, decreasing the photocurrent intensity of ITO/BiOBr/Bi_2S_3/PDA electrode (curve d). After modified with anti-SCCA and BSA, the photocurrent signal of electrode reduced due to the excellent insulation of biological macromolecule. By the specific recognition between SCCA and anti-SCCA, different concentrations of SCCA were modified on the ITO/BiOBr/Bi_2S_3/PDA/anti-SCCA/BSA electrode decreasing the photocurrent signal, which achieved the detection of SCCA.

In order to further illustrate the construction process of the PEC immunosensor, EIS of the modified electrodes were researched in [Fe(CN)$_6$]$^{3-/4-}$ solution (5.0 mmol L^{-1}, containing 0.10 mol L^{-1} KCl). As an effective method, EIS is used to describe the electron transfer resistance of electrode which changes with electrode modification. In general, the EIS consists of a semicircle part with higher frequency in the process of electron transfer restriction and a linear part with lower frequency during diffusion. And the semicircle diameter reflects the electron-transfer resistance (R_{et}) value, which represents the magnitude of resistance. As shown in Fig. 5B, the curve a exhibited the EIS of bare ITO electrode, and the diameter of semicircle was small due to the certain conductivity of ITO electrode. After modified with BiOBr (curve b) and Na_2S (curve c), the diameter of semicircle gradually increased proving the successful preparation of BiOBr/Bi_2S_3 on the ITO electrode. Subsequently, the diameter was decreased with the addition of DA (curve d). Because the DA adsorption is so strong that it may adsorb [Fe(CN)$_6$]$^{3-/4-}$ ions in the solution promoting the electron transfer and reducing the resistance of electron transfer. Then, the diameter of semicircle gradually increased with the modified of anti-SCCA (curve e), BSA (curve f) and SCCA (curve g), which was caused by the excellent insulativity of biological macromolecules blocking the electron transfer. Moreover, the Randles equivalent circuit for EIS was displayed in the inset in Fig. 5B consisting of the double layer capacitance (C_{dl}), the resistance of solution (R_s), the Warburg impedance (Z_w) and R_{et}. The relevant data were displayed in Table S3 (ESI†).

Fig. 5C displayed the schematic of electron transfer of the prepared PEC immunosensor. Under the irradiation of visible light, the band-gap of pure BiOBr was so wide (2.7 eV) that the e^- and h^+ were difficult to separate. The band-gap of Bi_2S_3 was 1.4 eV [33], which was benefit to the separation of e^-/h^+. Therefore, Na_2S was modified on the surface of BiOBr to obtain BiOBr/Bi_2S_3 heterostructures via self-sacrificial synthesis method. Under the irradiation of visible light, the electrons were

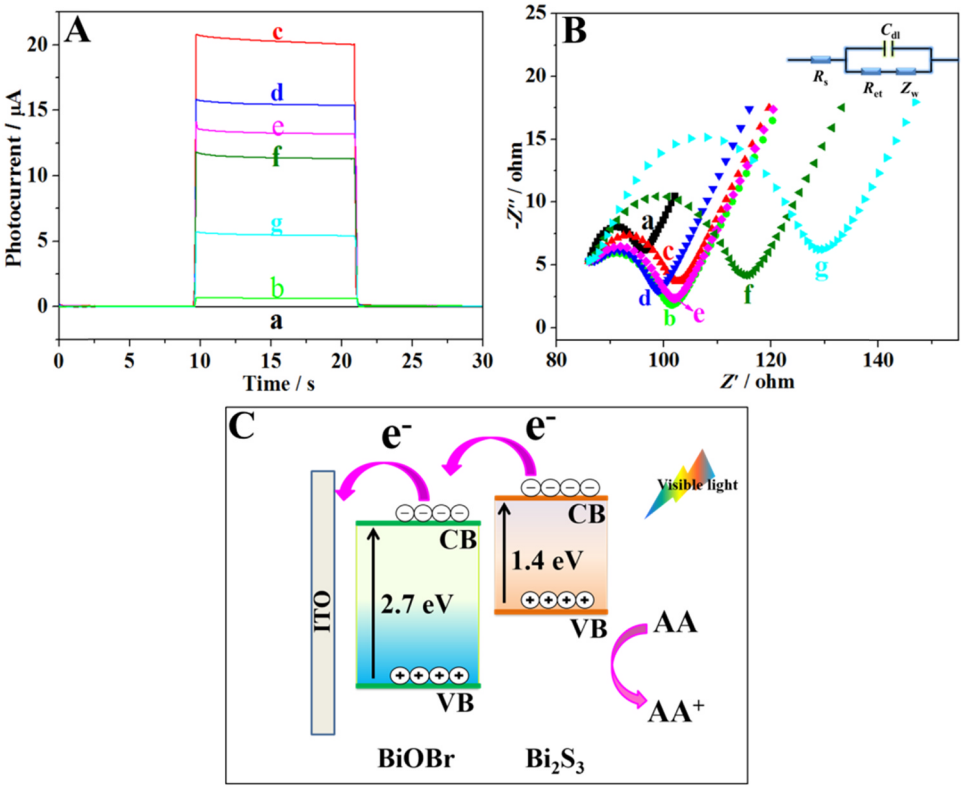

Fig. 5. (A) Time-based photocurrent response curves and (B) EIS Nyquist plots of (a) ITO, (b) ITO/BiOBr, (c) ITO/BiOBr/Bi_2S_3, (d) ITO/BiOBr/Bi_2S_3/PDA, (e) ITO/BiOBr/Bi_2S_3/PDA/anti-SCCA, (f) ITO/BiOBr/Bi_2S_3/PDA/anti-SCCA/BSA, (g) ITO/BiOBr/Bi_2S_3/PDA/anti-SCCA/BSA/SCCA. The inset in B was Randles equivalent circuit for EIS. The applied potential was 0 V. (C) The schematic of electron transfer of PEC immunosensor based on BiOBr/Bi_2S_3 in AA electrolyte, c_{SCCA} = 1 ng mL^{-1}.

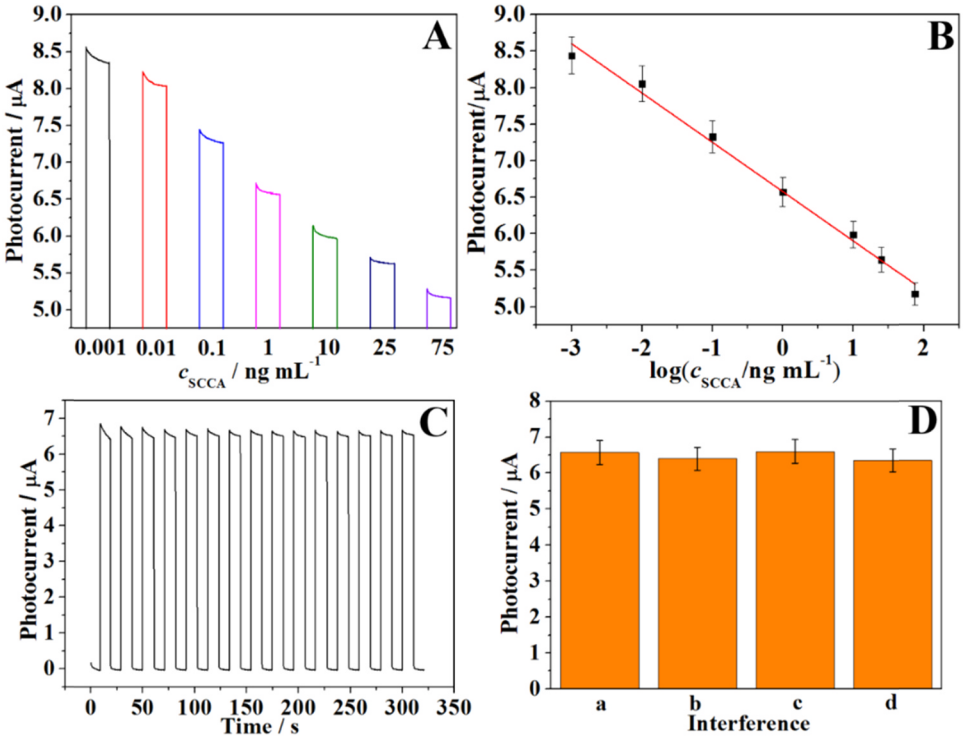

Fig. 6. (A) Photocurrent response curve and (B) the logarithmic calibration curve of the PEC immunosensor for the detection of different concentrations of SCCA. (C) Stability evaluation of the PEC immunosensor under on/off irradiation cycles for 320 s, c_{SCCA} = 1 ng mL^{-1}. (D) Selectivity detection of the PEC immunosensor for SCCA. 1 ng mL^{-1} SCCA (a), 1 ng mL^{-1} SCCA + 100 ng mL^{-1} CEA (b), 1 ng mL^{-1} SCCA + 100 ng mL^{-1} PSA (c), 1 ng mL^{-1} SCCA + 100 ng mL^{-1} HlgG (d). The applied potential was 0 V.

easily excited, and then efficiently transferred from the VB of Bi_2S_3 to CB. More importantly, the CB edge of Bi_2S_3 is higher than that of BiOBr accelerating the photo-generated electrons transfer to the CB of BiOBr. The wide band-gap of BiOBr was benefit to the electrons transfer from BiOBr to ITO to obtain distinguished photocurrent signal, which indicated the BiOBr/Bi_2S_3 heterostructures possessed satisfying photoelectric activity corresponding to the UV–vis diffuse reflectance spectra of BiOBr/Bi_2S_3 (shown in Fig. 3B). Meanwhile, AA was used as an electron donor clearing photo-generated holes to ensure the stability of photocurrent signals.

3.4. Sensitive PEC immunosensor detection of target SCCA

As shown in Fig. 6A, it was obvious that the photocurrent intensity gradually decreased with the increase of the concentration of SCCA. Because of the specific immune response between SCCA and anti-SCCA, different concentrations of SCCA were bound to blank electrodes (ITO/BiOBr/Bi_2S_3/PDA/anti-SCCA/BSA) to reduce the photocurrent signal, which showed the fabricated PEC immunosensor achieved sensitive detection for target SCCA. With the logarithm of SCCA concentration range from 0.001 ng mL^{-1} to 75 ng mL^{-1}, the photocurrent intensity reduced linearly (Fig. 6B). And the linear equation was I = 6.577–0.675 log (c_{SCCA}, ng·mL^{-1}) with a correlation coefficient of 0.990. According to the literature [34], the detection limit was 0.3 pg mL^{-1} (S/N = 3). As displayed in Table S4 (ESI†), the fabricated PEC immunosensor achieves much lower detection limit and wider detection linear range than other detection methods.

Modified with 1 ng mL^{-1} SCCA, the stability of the prepared PEC immunosensor was researched under on/off irradiation cycles for 320 s (shown in Fig. 6C). There was no noticeable variation in the photocurrent signal, which manifested the fabricated PEC immunosensor possessed excellent stability. Meanwhile, the reproducibility of the PEC immunosensor (modified with 1 ng mL^{-1} SCCA) was explored by measuring the photocurrent signals of five electrodes. The data were 6.85 μA, 6.51 μA, 7.03 μA, 6.43 μA and 6.47 μA, severally. And the relative standard deviation (RSD) was 4.0%, which manifested that the reproducibility of the PEC immunosensor was satisfying.

In addition, Fig. 6D showed the selectivity detection of the PEC immunosensor for SCCA. When modified 1 ng mL^{-1} SCCA solution (containing 100 ng mL^{-1} interfering substances) on the blank electrodes, the photocurrent signal was no obvious variation comparing with that of the SCCA solution absent of interfering substances. The result illustrated the prepared PEC immunosensor owned excellent selectivity and specificity to detect SCCA.

3.5. Application of the fabricated PEC immunosensor in human serum

In order to explore the application of the fabricated PEC immunosensor, the recoveries of SCCA in human serum were detected. The related data were shown in Table S5 (ESI†), the RSD was obtained between 2.26% and 4.18% and the recovery was in the range from 92.0% to 102%. Thus, the prepared PEC immunosensor have promising practical application for SCCA detection.

4. Conclusion

In our work, a novel visible light PEC immunosensor based on BiOBr/Bi_2S_3 heterostructures was fabricated successfully for SCCA detection. With hierarchical structure, BiOBr microspheres had the larger specific surface contributing to the combination with more particles. By the self-sacrificial synthesis method, Bi_2S_3 nanoparticles formed on the BiOBr microflowers to obtain BiOBr/Bi_2S_3 composites. The BiOBr/Bi_2S_3 revealed the satisfying absorption to visible light, which enhanced the photocurrent signal of the fabricated PEC immunosensor. Moreover, the PEC immunosensor was successfully prepared based on the specific recognition between antigen and antibody under the ideal condition, which realized the ultrasensitive determination of SCCA.

Acknowledgments

The National Natural Science Foundation of China (No. 21775054, 21675063, 21575050), the Natural Science Foundation of Shandong Province (Grant No. ZR2017BB030, ZR2016JL013, ZR2017MB027), and QW thanks the Special Foundation for Taishan Scholar Professorship of Shandong Province (No. ts20130937) and UJN.

Appendix A. Supporting information

Supplementary data associated with this article can be found in the online version at doi:10.1016/j.talanta.2019.02.043.

References

[1] W.W. Tong, G.H. Tong, J. Wang, X.S. Qin, L.U. Li-Ping, Y. Liu, Value of CYFRA21-1,NSE,CRP and SCCA in diagnosis of lung cancer, Chin. J. Immunol. (2015).

[2] W. Zhao, H. Yu, Z. Han, N. Gao, J. Xue, Y. Wang, Clinical significance of joint detection of serum CEA, SCCA, and bFGF in the diagnosis of lung cancer, Int. J. Clin. Exp. Pathol. 8 (2015) 9506–9511.

[3] Y. Li, Y. Zhang, F. Li, J. Feng, M. Li, L. Chen, Y. Dong, Ultrasensitive electrochemical immunosensor for quantitative detection of SCCA using Co_3O_4@CeO_2-Au@Pt nanocomposite as enzyme-mimetic labels, Biosens. Bioelectron. 92 (2017) 33–39.

[4] L. Wu, Y. Hu, Y. Sha, W. Li, T. Yan, S. Wang, X. Li, Z. Guo, J. Zhou, X. Su, An "in-electrode"-type immunosensing strategy for the detection of squamous cell carcinoma antigen based on electrochemiluminescent AuNPs/g-C_3N_4 nanocomposites, Talanta 160 (2016) 247–255.

[5] X. Ye, M. Li, Y. Hu, Z. Wang, Y. Wang, H. Deng, X. Xiong, C. Li, D. Sun, Sensitive photoelectrochemical immunosensor for squamous cell carcinoma antigen based on $MoSe_2$ nanosheets and hollow gold nanospheres, Sens. Actuators B 275 (2018) 199–205.

[6] Y. Lin, Q. Zhou, D. Tang, Dopamine-loaded liposomes for in-situ amplified photoelectrochemical immunoassay of AFB_1 to enhance photocurrent of Mn^{2+}-doped $Zn_3(OH)_2V_2O_7$ nanobelts, Anal. Chem. 89 (2017) 11803–11810.

[7] D. Jiang, X. Du, L. Zhou, H. Li, K. Wang, New insights toward efficient charge-separation mechanism for high-performance photoelectrochemical aptasensing: enhanced charge-carrier lifetime via coupling ultrathin MoS_2 nanoplates with nitrogen-doped graphene quantum dots, Anal. Chem. 89 (2017) 4525–4531.

[8] C. Wang, X. Ye, Z. Wang, T. Wu, Y. Wang, C. Li, Molecularly imprinted photoelectrochemical sensor for human epididymis protein 4 based on polymerized ionic liquid hydrogel and gold nanoparticle/ZnCdHgSe quantum dots composite film, Anal. Chem. 89 (2017) 12391–12398.

[9] P. Yan, D. Jiang, Y. Tian, L. Xu, J. Qian, H. Li, J. Xia, H. Li, A sensitive signal-on photoelectrochemical sensor for tetracycline determination using visible-light-driven flower-like CN/BiOBr composites, Biosens. Bioelectron. 111 (2018) 74–81.

[10] D. Fan, C. Bao, M.S. Khan, C. Wang, Y. Zhang, Q. Liu, X. Zhang, Q. Wei, A novel label-free photoelectrochemical sensor based on N,S-GQDs and CdS co-sensitized hierarchical Zn_2SnO_4 cube for detection of cardiac troponin I, Biosens. Bioelectron. 106 (2018) 14–20.

[11] X. Li, X. Wang, T. Fang, L. Zhang, J. Gong, Disposable photoelectrochemical sensing strip for highly sensitive determination of perfluorooctane sulfonyl fluoride on functionalized screen-printed carbon electrode, Talanta 181 (2018) 147–153.

[12] Z. Fan, L. Fan, S. Shuang, C. Dong, Highly sensitive photoelectrochemical sensing of bisphenol A based on zinc phthalocyanine/TiO_2 nanorod arrays, Talanta 189 (2018) 16–23.

[13] H. Ye, H. Wang, B. Zhang, F. Zhao, B. Zeng, Tremella-like $ZnIn_2S_4$/graphene composite based photoelectrochemical sensor for sensitive detection of dopamine, Talanta 186 (2018) 459–466.

[14] S.R. Zhu, Q. Qi, W.N. Zhao, Y. Fang, L. Han, Enhanced photocatalytic activity in hybrid composite combined BiOBr nanosheets and Bi_2S_3 nanoparticles, J. Phys. Chem. Solids 121 (2018) 163–171.

[15] J. Hu, C. Zhai, C. Yu, L. Zeng, Z. Liu, M. Zhu, Visible light-enhanced electrocatalytic alcohol oxidation based on two dimensional Pt-BiOBr nanocomposite, J. Colloid Interface Sci. 524 (2018) 195–203.

[16] R. Li, H. Ren, W. Ma, S. Hong, L. Wu, Y. Huang, Synthesis of BiOBr microspheres with ethanol as self-template and solvent with controllable morphology and photocatalytic activity, Catal. Commun. 106 (2018) 1–5.

[17] H. Yu, B. Huang, H. Wang, X. Yuan, L. Jiang, Z. Wu, J. Zhang, G. Zeng, Facile construction of novel direct solid-state Z-scheme AgI/BiOBr photocatalysts for highly effective removal of ciprofloxacin under visible light exposure: mineralization efficiency and mechanisms, J. Colloid Interface Sci. 522 (2018) 82–94.

[18] M. Du, Y. Du, Y. Feng, K. Yang, X. Lv, N. Jiang, Y. Liu, Facile preparation of BiOBr/cellulose composites by in situ synthesis and its enhanced photocatalytic activity under visible-light, Carbohydr. Polym. 195 (2018) 393–400.

[19] W. Guo, Q. Qin, G. Lei, D. Wang, Y. Guo, Y. Yang, Morphology-controlled preparation and plasmon-enhanced photocatalytic activity of Pt–BiOBr heterostructures, J. Hazard. Mater. 308 (2016) 374–385.

[20] Y. Guo, Y. Zhang, N. Tian, H. Huang, Homogeneous {001}-BiOBr/Bi heterojunctions: facile controllable synthesis and morphology-dependent photocatalytic activity, ACS Sustain. Chem. Eng. 4 (2016) 4003–4012.

[21] T. Hu, Y. Yang, K. Dai, J. Zhang, C. Liang, A novel Z-scheme Bi_2MoO_6/BiOBr photocatalyst for enhanced photocatalytic activity under visible light irradiation, Appl. Surf. Sci. 456 (2018) 473–481.

[22] J. Di, J. Xia, M. Ji, B. Wang, X. Li, Q. Zhang, Z. Chen, H. Li, Nitrogen-doped carbon quantum dots/BiOBr ultrathin nanosheets: in situ strong coupling and improved molecular oxygen activation ability under visible light irradiation, ACS Sustain. Chem. Eng. 4 (2016) 136–146.

[23] S. Adhikari, D.-H. Kim, Synthesis of Bi_2S_3/Bi_2WO_6 hierarchical microstructures for enhanced visible light driven photocatalytic degradation and photoelectrochemical sensing of ofloxacin, Chem. Eng. J. 354 (2018) 692–705.

[24] B. Zhang, X. Ye, W. Hou, Y. Zhao, Y. Xie, Biomolecule-assisted synthesis and electrochemical hydrogen storage of Bi_2S_3 flowerlike patterns with well-aligned nanorods, J. Phys. Chem. B 110 (2006) 8978–8985.

[25] Z. Yang, Y. Wang, D. Zhang, C. Chen, A sensitizing photoelectrochemical sensing platform strategy based on bio-etching preparation of Bi_2S_3/BiOCl p–n heterojunction, Talanta 190 (2018) 357–362.

[26] Y. Wang, J. Jin, W. Chu, D. Cahen, T. He, Synergistic effect of charge generation and separation in epitaxially grown BiOCl/Bi_2S_3 nano-heterostructure, ACS Appl. Mater. Interfaces 10 (2018) 15304–15313.

[27] R. Wang, G. Cheng, Z. Dai, J. Ding, Y. Liu, R. Chen, Ionic liquid-employed synthesis of Bi_2E_3 (E = S, Se, and Te) hierarchitectures: the case of Bi_2S_3 with superior visible-light-driven Cr(VI) photoreduction capacity, Chem. Eng. J. 327 (2017) 371–386.

[28] D.V. Freitas, J.R. González-Moya, T.A.S. Soares, R.R. Silva, D.M. Oliveira, H.S. Mansur, G. Machado, M. Navarro, Enhanced visible-light photoelectrochemical conversion on TiO_2 nanotubes with Bi_2S_3 quantum dots obtained by in situ electrochemical method, ACS Appl. Energy Mater. 1 (2018) 3636–3645.

[29] H. Cheng, B. Huang, P. Wang, Z. Wang, Z. Lou, J. Wang, X. Qin, X. Zhang, Y. Dai, In situ ion exchange synthesis of the novel Ag/AgBr/BiOBr hybrid with highly efficient decontamination of pollutants, Chem. Commun. 47 (2011) 7054–7056.

[30] D.N. Xiong, G.F. Huang, B.X. Zhou, Q. Yan, A.L. Pan, W.Q. Huang, Facile ion-exchange synthesis of mesoporous Bi_2S_3/ZnS nanoplate with high adsorption capability and photocatalytic activity, J. Colloid Interface Sci. 464 (2016) 103–109.

[31] M. Zhu, Q. Liu, W. Chen, Y. Yin, L. Ge, H. Li, K. Wang, Boosting the visible-light photoactivity of BiOCl/$BiVO_4$/N-GQDs ternary heterojunctions based on an internal z-scheme charge transfer of N-GQDs: simultaneous bandgap narrowing and carrier lifetime prolonging, ACS Appl. Mater. Interfaces 9 (2017) 38832–38841.

[32] J. Feng, Y. Li, Z. Gao, H. Lv, X. Zhang, Y. Dong, P. Wang, D. Fan, Q. Wei, A competitive-type photoelectrochemical immunosensor for aflatoxin B1 detection based on flower-like WO_3 as matrix and Ag_2S-enhanced $BiVO_4$ for signal amplification, Sens. Actuators B 270 (2018) 104–111.

[33] J. Cao, B. Xu, H. Lin, B. Luo, S. Chen, Novel Bi_2S_3-sensitized BiOCl with highly visible light photocatalytic activity for the removal of rhodamine B, Catal. Commun. 26 (2012) 204–208.

[34] K. Ren, J. Wu, F. Yan, Y. Zhang, H. Ju, Immunoreaction-triggered DNA assembly for one-step sensitive ratiometric electrochemical biosensing of protein biomarker, Biosens. Bioelectron. 66 (2015) 345–349.